ISSN 1063-7761, Journal of Experimental and Theoretical Physics, 2008, Vol. 106, No. 2, pp. 380–387. © Pleiades Publishing, Inc., 2008.
Original Russian Text © S.P. Kuznetsov, 2008, published in Zhurnal Éksperimental'noĭ i Teoreticheskoĭ Fiziki, 2008, Vol. 133, No. 2, pp. 438–446.

STATISTICAL, NONLINEAR, AND SOFT MATTER PHYSICS

On the Feasibility of a Parametric Generator of Hyperbolic Chaos

S. P. Kuznetsov

Saratov Branch, Institute of Radio Engineering and Electronics, Russian Academy of Sciences, Saratov, 410019 Russia
e-mail: spkuz@rambler.ru

Received May 16, 2007

Abstract—A chaos generator consisting of two subsystems is considered. Each subsystem is a pair of parametrically coupled oscillators whose free-running frequencies differ by a factor of two. The subsystems are alternately driven by the third harmonic of a basic frequency, and energy is transferred between them through signal squarers. Based on a qualitative analysis and numerical results, a hypothesis is put forward that the system implements a hyperbolic strange attractor.

PACS numbers: 05.45.-a
DOI: 10.1134/S1063776108020167

1. INTRODUCTION

In the mathematical theory of dynamical systems [1–11], uniformly hyperbolic chaotic attractors are defined as invariant sets where all orbits are of saddle type. They are structurally stable; i.e., the attractor structure is robust under changes in control-parameter values. These strange attractors have strong chaotic properties amenable to far-reaching mathematical analysis. However, uniformly hyperbolic chaotic attractors are not characteristic of a vast majority of real systems exhibiting complex behavior. The examples of hyperbolic attractors discussed in textbooks and monographs on nonlinear dynamics, such as Plykin's attractor or Smale–Williams solenoid, are constructed by using artificial mathematical models [1–11].

Recently, a nonautonomous physical system was proposed that combines two van der Pol oscillators [12–14] and exhibits a Smale–Williams strange attractor in the Poincaré map. In [15, 16], a numerical verification of sufficient conditions for the existence of a hyperbolic attractor, known from the literature [1, 6], was performed for this system.

Other systems of this kind using autonomous and nonautonomous oscillators were discussed in [16–19]. The general principle that underlies the operation of these systems is phase manipulation performed as signals are transferred between alternately excited oscillators, so that the evolution of the phase variable corresponds to an iterative chaotic map.

This principle is conveniently implemented in parametrically driven systems, which are widely used in theory and applications [20–23]. The physical processes employed in such a system may belong to the realm of electronics, mechanics, acoustics, or nonlinear optics.

In a commonly used type of parametric generator, two oscillators are coupled by a reactive coupling element characterized by a time-varying parameter. The free-running oscillator frequencies ω_1 and ω_2 are related to the driving frequency ω_3 by the parametric resonance condition $\omega_1 + \omega_2 = \omega_3$. Both oscillators are excited simultaneously, and the oscillations can be stabilized, in particular, by introducing a nonlinear damping.

Consider a system consisting of parametric generators A and B of this type, as schematized in Fig. 1. In each subsystem, the free-running frequencies of the parametrically coupled oscillators are such that $\omega_2 = 2\omega_1$ and $\omega_3 = 3\omega_1$; i.e., parametric resonance conditions

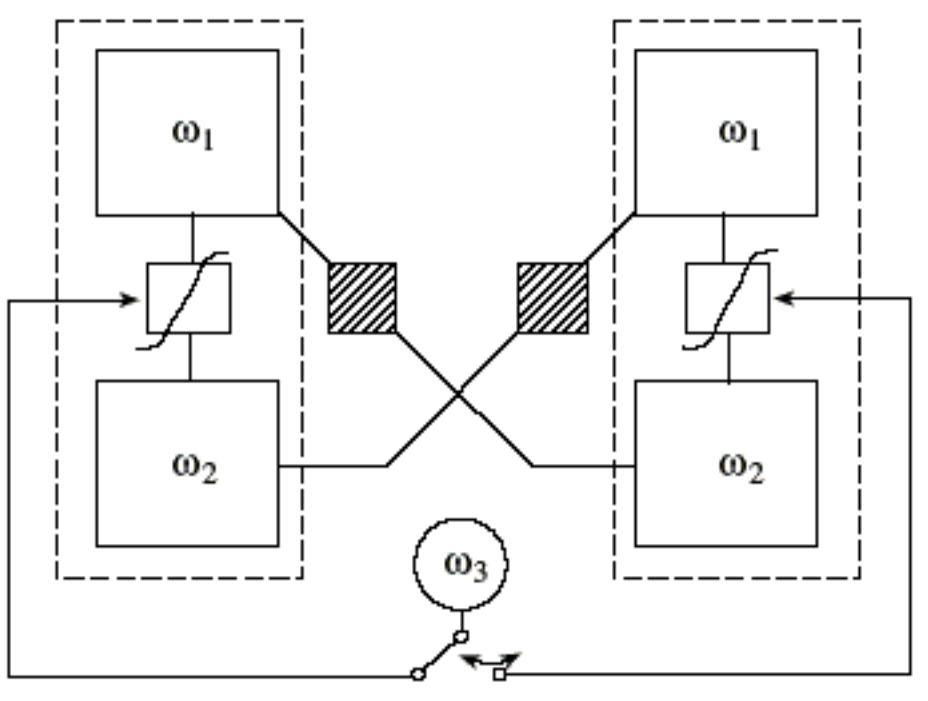

Fig. 1. Parametric chaos generator block diagram. Blocks labeled as ω_1 and ω_2 represent the respective oscillators with these free-running frequencies; those labeled with a waveform, reactive coupling elements characterized by a parameter oscillating at the driving carrier frequency ω_3; hatched squares, signal squarers.

are obviously satisfied. The oscillator of frequency ω_1 is coupled to the oscillator of frequency ω_2 in the other subsystem by a signal squarer. By virtue of the assumed relation between the frequencies, the second harmonic of one oscillator resonantly drives the other oscillator.

The subsystems are driven in turn so that parametrically excited oscillations grow and decay alternately in both subsystems. Each excitation of a subsystem is triggered by a second harmonic signal generated by the other subsystem. The oscillation phase is doubled by each signal transfer so that it is multiplied by a factor of 4 over a period of driving-signal modulation. As a result, the system generates, with the modulation period, a sequence of pulses whose carrier phase chaotically varies from pulse to pulse.

Hypothetically, the chaotic attractor corresponding to any particular set of parameter values for which the phases evolve as described above can be classified as uniformly hyperbolic. More precisely, the attractor generated by the map that determines the change in the system's state over a modulation period is of Smale–Williams solenoid type.

In the system proposed here, the phase manipulation is performed as energy is transferred between oscillators, whereas the key role in the systems discussed in [12–19] is played by a non-oscillatory external source of energy that compensates for oscillator losses, rather than by energy transfer.

2. GENERATOR MODEL: GOVERNING EQUATIONS AND PRINCIPLE OF OPERATION

Consider the system described by the Lagrangian

$$L = \frac{1}{2}(\dot{x}_1^2 + \dot{x}_2^2 + \dot{y}_1^2 + \dot{y}_2^2 - \omega_1^2 x_1^2 - \omega_2^2 x_2^2 - \omega_1^2 y_1^2 - \omega_2^2 y_2^2) + \kappa[x_1 x_2 f(t) + y_1 y_2 g(t)] \times \sin\omega_3 t + \varepsilon(x_1^2 y_2 + y_1^2 x_2), \quad (1)$$

where $x_{1,2}$ and $y_{1,2}$ are the generalized coordinates of two coupled pairs of oscillators, $\dot{x}_{1,2}$ and $\dot{y}_{1,2}$ are the corresponding generalized velocities, and ω_1 and $\omega_2 = 2\omega_1$ are the respective free-running oscillator frequencies in both pairs. The parameter κ quantifies the driving-signal strength, and the functions $f(t)$ and $g(t)$ determine the respective slowly varying amplitudes, of the signals with the carrier frequency $\omega_3 = \omega_1 + \omega_2 = 3\omega_1$ that drive the two pairs of oscillators. The parameter ε is the coupling strength between oscillators belonging to different pairs.

The nonlinear damping required for saturation of parametric instability and existence of an attractor is introduced by using the Rayleigh dissipation function [24] defined as follows:

$$R = \frac{1}{2}(\alpha_1\dot{x}_1^2 + \alpha_2\dot{x}_2^2 + \alpha_1\dot{y}_1^2 + \alpha_1\dot{y}_2^2) + \frac{1}{4}(\beta_1\dot{x}_1^4 + \beta_2\dot{x}_2^4 + \beta_1\dot{y}_1^4 + \beta_1\dot{y}_2^4), \quad (2)$$

where $\alpha_{1,2}$ and $\beta_{1,2}$ are positive constant parameters. The equations of motion for the system [24],

$$\frac{d}{dt}\left(\frac{\partial L}{\partial \dot{x}_i}\right) = \frac{\partial L}{\partial x_i} - \frac{\partial R}{\partial \dot{x}_i}, \qquad \frac{d}{dt}\left(\frac{\partial L}{\partial \dot{y}_i}\right) = \frac{\partial L}{\partial y_i} - \frac{\partial R}{\partial \dot{y}_i}, \quad i = 1, 2, \quad (3)$$

are then written as

$$\begin{aligned}
\ddot{x}_1 + \omega_1^2 x_1 &= \kappa x_2 f(t)\sin\omega_3 t \\
&+ 2\varepsilon x_1 y_2 - \alpha_1\dot{x}_1 - \beta_1\dot{x}_1^3, \\
\ddot{x}_2 + \omega_2^2 x_2 &= \kappa x_1 f(t)\sin\omega_3 t \\
&+ \varepsilon y_1^2 - \alpha_2\dot{x}_2 - \beta_2\dot{x}_2^3, \\
\ddot{y}_1 + \omega_1^2 y_1 &= \kappa y_2 g(t)\sin\omega_3 t \\
&+ 2\varepsilon y_1 x_2 - \alpha_1\dot{y}_1 - \beta_1\dot{x}_1^3, \\
\ddot{y}_2 + \omega_2^2 y_2 &= \kappa y_1 g(t)\sin\omega_3 t \\
&+ \varepsilon x_1^2 - \alpha_2\dot{y}_2 - \beta_2\dot{y}_2^3.
\end{aligned} \quad (4)$$

The amplitude functions $f(t)$ and $g(t)$ are defined so that the driving signals are slowly modulated in antiphase:

$$f(t) = \sin^2(\pi t/T), \quad g(t) = \cos^2(\pi t/T). \quad (5)$$

The modulation period is a multiple of the driving-signal carrier period: $T = 2\pi N/\omega_3$, where N is an integer.[1]

When $N \gg 1$, the slowly varying amplitude method [21–23] can be used by setting

$$\begin{aligned}
x_1 &= A_1\exp(i\omega_1 t) + A_1^*\exp(-i\omega_1 t), \\
x_2 &= A_2\exp(i\omega_2 t) + A_2^*\exp(-i\omega_2 t), \\
y_1 &= B_1\exp(i\omega_1 t) + B_1^*\exp(-i\omega_1 t), \\
y_2 &= B_2\exp(i\omega_2 t) + B_2^*\exp(-i\omega_2 t),
\end{aligned} \quad (6)$$

[1] This condition implies that (4) is a system of equations with T-periodic coefficients. Therefore, the system's dynamics can be represented by the stroboscopic Poincaré map using sections of the extended phase space with time step T. However, this condition can be ignored here since Eqs. (8) for slowly varying amplitudes are used in the present analysis.

where $A_{1,2}(t) = A'_{1,2} + iA''_{1,2}$ and $B_{1,2}(t) = B'_{1,2} + iB''_{1,2}$ are slowly varying complex functions of time subject to the conditions

$$\begin{aligned}
\dot{A}_1\exp(i\omega_1 t) + \dot{A}_1^*\exp(-i\omega_1 t) &= 0,\\
\dot{A}_2\exp(i\omega_2 t) + \dot{A}_2^*\exp(-i\omega_2 t) &= 0,\\
\dot{B}_1\exp(i\omega_1 t) + \dot{B}_1^*\exp(-i\omega_1 t) &= 0,\\
\dot{B}_2\exp(i\omega_2 t) + \dot{B}_2^*\exp(-i\omega_2 t) &= 0.
\end{aligned} \tag{7}$$

Substituting these relations into (4), multiplying the equations for A_1 and B_1 by $\exp(-i\omega_1 t)$ and A_2 and B_2 by $\exp(-i\omega_2 t)$, averaging the resulting equations over the carrier period, and using the assumed relation between $\omega_{1,2,3}$, we obtain

$$\begin{aligned}
\dot{A}_1 &= -\frac{\kappa}{4\omega_1}f(t)A_2^* - i\frac{\varepsilon}{\omega_1}A_1^*B_2\\
&\quad -\frac{1}{2}\alpha_1 A_1 - \frac{3}{2}\omega_1^2\beta_1 A_1|A_1|^2,\\
\dot{A}_2 &= -\frac{\kappa}{4\omega_2}f(t)A_1^* - i\frac{\varepsilon}{2\omega_2}B_1^2\\
&\quad -\frac{1}{2}\alpha_2 A_2 - \frac{3}{2}\omega_2^2\beta_2 A_2|A_2|^2,\\
\dot{B}_1 &= -\frac{\kappa}{4\omega_1}g(t)B_2^* - i\frac{\varepsilon}{\omega_1}B_1^*A_2\\
&\quad -\frac{1}{2}\alpha_1 B_1 - \frac{3}{2}\omega_1^2\beta_1 B_1|B_1|^2,\\
\dot{B}_2 &= -\frac{\kappa}{4\omega_2}g(t)B_1^* - i\frac{\varepsilon}{2\omega_2}A_1^2\\
&\quad -\frac{1}{2}\alpha_2 B_2 - \frac{3}{2}\omega_2^2\beta_2 B_2|B_2|^2.
\end{aligned} \tag{8}$$

If $\varepsilon = 0$, the system splits into isolated subsystems A and B, each comprising two parametrically coupled oscillators. To be specific, consider subsystem A. (The other subsystem is analyzed analogously.) For the undamped subsystem with $f(t) \equiv 1$, the complex amplitudes are governed by the equations

$$\dot{A}_1 = -\frac{\kappa}{4\omega_1}A_2^*, \quad \dot{A}_2 = -\frac{\kappa}{4\omega_2}A_1^*.$$

Their general solution is

$$A_1 = C_+\exp\left(\frac{\kappa t}{4\sqrt{\omega_1\omega_2}}\right) + C_-\exp\left(-\frac{\kappa t}{4\sqrt{\omega_1\omega_2}}\right),$$

$$A_2 = -\sqrt{\frac{\omega_2}{\omega_1}}\left[C_+^*\exp\left(\frac{\kappa t}{4\sqrt{\omega_1\omega_2}}\right) + C_-^*\exp\left(-\frac{\kappa t}{4\sqrt{\omega_1\omega_2}}\right)\right],$$

where $C_+ = R\exp(i\varphi)$ and $C_- = R\exp(-i\varphi)$ are complex constants determined by the initial conditions. Since the second terms decay, we obtain the long-time asymptotic expressions

$$A_1 \approx C_+\exp\left(\frac{\kappa t}{4\sqrt{\omega_1\omega_2}}\right),$$

$$A_2 \approx -\sqrt{\frac{\omega_2}{\omega_1}}C_+^*\exp\left(\frac{\kappa t}{4\sqrt{\omega_1\omega_2}}\right);$$

i.e.,

$$x_1 \approx 2R\exp\left(\frac{\kappa t}{4\sqrt{\omega_1\omega_2}}\right)\cos(\omega_1 t + \varphi),$$

$$x_2 \approx -2R\sqrt{\frac{\omega_2}{\omega_1}}\exp\left(\frac{\kappa t}{4\sqrt{\omega_1\omega_2}}\right)\cos(\omega_2 t - \varphi).$$

Thus, the parametrically excited oscillations at the first and second harmonics of ω_1 are phase-shifted by a constant φ depending on the initial conditions. When the nonlinear damping is taken into account, the oscillation amplitude saturates, yet the phase relation is preserved.

Now, consider the regime when the coupled subsystems A and B (with nonzero ε) are driven in turn.

In each subsystem, the oscillator with free-running frequency $\omega_2 = 2\omega_1$ is excited by the second harmonic of the oscillator with free-running frequency ω_1, produced by a signal squarer. The double phase shift in the second harmonic[2] passes to the excited oscillator. During the next modulation half-period, the subsystems A and B play reverse roles, and the phase shift of the passed signal doubles once again. Thus, the phase shift after a modulation period can be approximately represented by the map $\varphi_{new} = 4\varphi_{old} + \text{const} \pmod{2\pi}$. It is a Bernoulli-type map [25] with chaotic dynamics characterized by the Lyapunov exponent $\Lambda = \ln 4 \approx 1.386$.

The discrete-time evolution of the system is described by the stroboscopic Poincaré map obtained by sampling the system's 8D state vectors $\mathbf{X}_n$ at times

[2] Indeed, by a well-known trigonometric identity, we have $\cos^2(\omega_1 t + \varphi) = \frac{1}{2}\cos(2\omega_1 t + 2\varphi) + \text{off-resonant term}$.

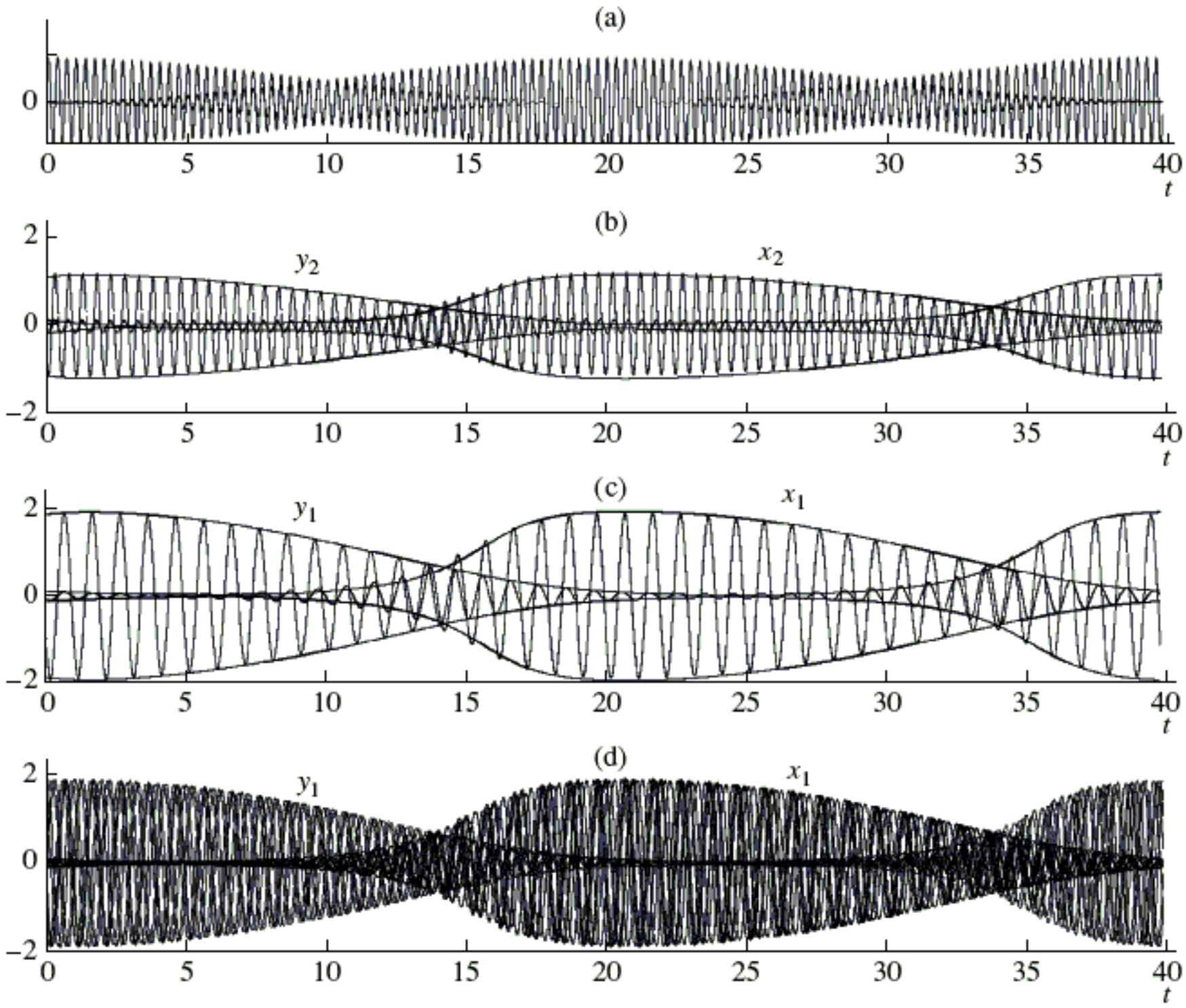

Fig. 2. Time-domain waveforms obtained by computing Eqs. (4) with parameter values (10) to illustrate irregular (virtually chaotic) behavior: (a) driving signal; (b, c) single samples; (d) eight superimposed samples of the same signal realization. The envelopes in panels (b) and (c) are obtained by numerical solution of Eqs. (8) for complex amplitudes.

$t_n = nT$. Solving Eqs. (4) or (8) on a time interval T starting from a particular t_n, we obtain a new state vector $\mathbf{X}_{n+1}$. The function

$$\mathbf{X}_{n+1} = \mathbf{T}(\mathbf{X}_n), \tag{9}$$

which maps the 8D phase space into itself, is the stroboscopic Poincaré map associated with a system of differential evolution equations whose right-hand sides are smooth and bounded on a bounded region in the phase space. By virtue of the existence, uniqueness, continuity, and differentiability of the solution to the system, $\mathbf{T}$ is a diffeomorphism (a smooth map with a smooth inverse [26]). To define the phase φ, consider the oscillator with free-running frequency ω_1 in the subsystem active at t_n. In the 8D phase space, the eigendirection associated with the phase $\varphi_{n+1} = 4\varphi_n + \text{const} \pmod{2\pi}$ is expanding and the remaining seven directions are contracting (see below).

3. CHAOTIC DYNAMICS: NUMERICAL RESULTS

The system's dynamics are simulated for $\omega_1 = 2\pi$, $\omega_2 = 4\pi$, and $\omega_3 = 6\pi$; i.e., time is measured in units of the shortest free-running oscillator period.

Figure 2 shows modulation-period-long samples of steady-state x and y waveforms, with modulated amplitudes (5) of the driving signals illustrated by Fig. 2a, computed by solving Eqs. (4) with the fourth-order Runge–Kutta method for

$$\begin{gathered} T = 40, \quad \varepsilon = 0.5, \quad \kappa = 35, \\ \alpha_1 = \alpha_2 = 0.6, \quad \beta_1 = \beta_2 = 0.01. \end{gathered} \tag{10}$$

It is clear that energy is alternately transferred between the subsystems in phase lock with the driving-signal modulation. The waveform generated by each subsystem is a pulse train modulating a high-frequency carrier with the driving-signal modulation period. However, the waveform is not strictly periodic: the carrier phase varies irregularly from pulse to pulse. A good qualitative illustration of this behavior is provided by Fig. 2d, which shows eight superimposed signal sam-

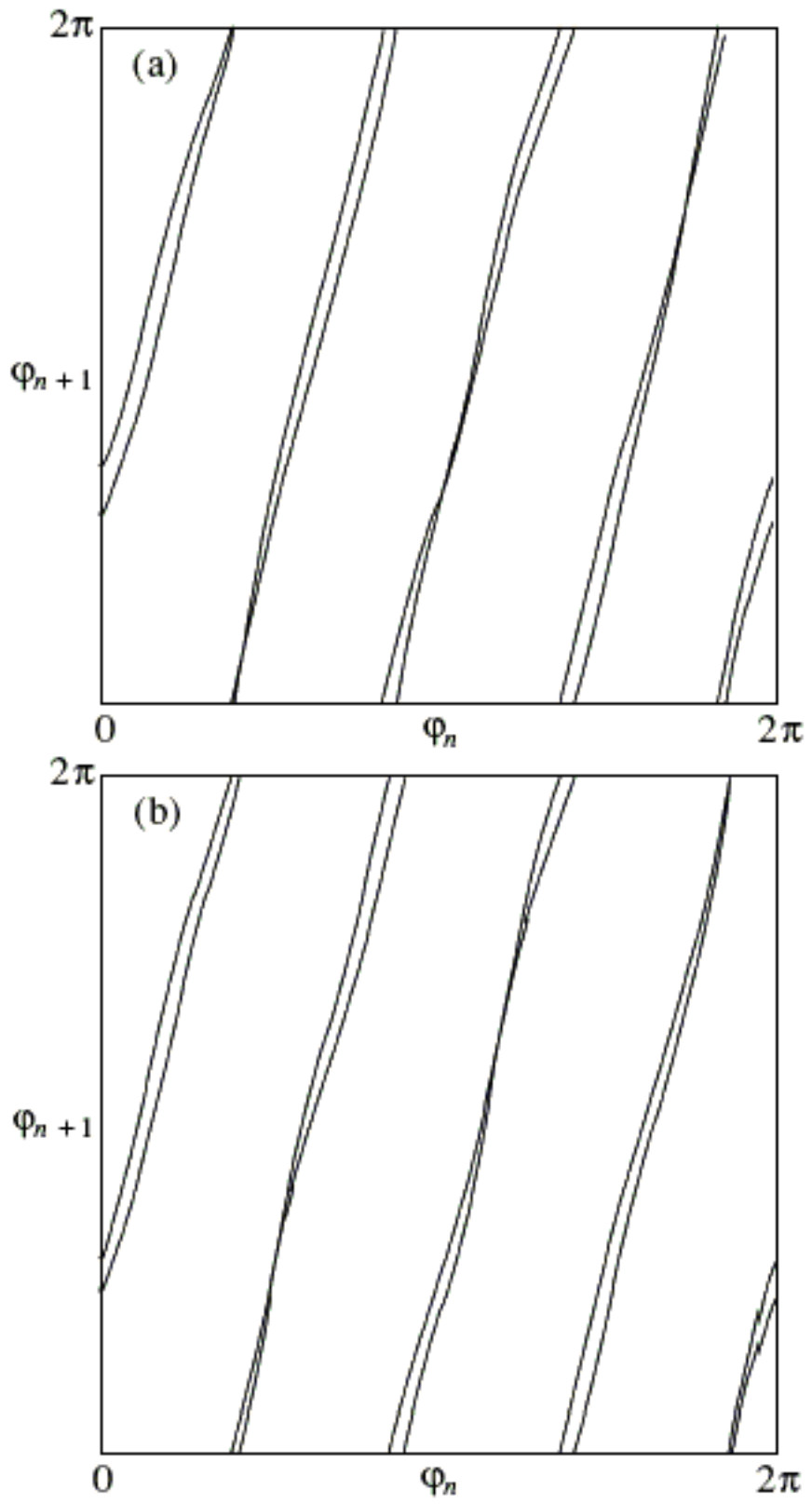

Fig. 3. First-return maps for the phase of an active subsystem obtained by computing Eqs. (4) (a) and Eqs. (8) for complex amplitudes (b) with parameter values (10).

ples corresponding to successive modulation periods. Figures 2b and 2c illustrate the time dependence of the oscillator amplitudes obtained by computing Eqs. (8) for slowly varying amplitudes. To correlate the waveforms, the initial conditions set at the starting point in time are calculated for the corresponding state of system (4) by using relations (6) and (7). The figure demonstrates good agreement between the results obtained by the slowly varying amplitude method and the exact solution.

First-return maps for the phase of the signal generated by subsystem B are shown in Fig. 3. Here, the abscissa and ordinate are the respective phases at $t_n = nT$ and t_{n+1}. The plots in Figs. 3a and 3b are obtained by computing Eqs. (4) and Eqs. (8) and calculating the phase as

$$\varphi_n = \arg[y_1(t_n) + \dot{y}_1(t_n)/i\omega_1]$$

and

$$\varphi_n = \arg B_1(t_n),$$

respectively. Note that the phase is defined only within an active time interval of the subsystem (when the output amplitude does not approach zero).[3] According to Fig. 3, as φ_n varies from 0 to 2π, the phase φ_{n+1} traverses the unit circle four times; i.e., the first-return map is topologically equivalent to the Bernoulli-type map $\varphi_{new} = 4\varphi_{old}$. The minor variability from period to period appears to be unimportant and can be neglected.

Since good agreement is demonstrated between the results obtained by computing the original and the amplitude equations, the analysis below is restricted to the amplitude equations.

Quantitative evidence of chaotic behavior is obtained by calculating Lyapunov exponents. To find the Lyapunov spectrum by Bennetin's algorithm [27, 28], Eqs. (8) are computed simultaneously with eight sets of equations for perturbations,

$$\begin{aligned}
\delta\dot{A}_1 &= -\frac{\kappa}{4\omega_1}f(t)\delta A_2^* - i\frac{\varepsilon}{\omega_1}(\delta A_1^* B_2 + A_1^*\delta B_2)\\
&-\frac{1}{2}\alpha_1\delta A_1 - \frac{3}{2}\omega_1^2\beta_1 A_1^2\delta A_1^* - 3\omega_1^2\beta_1 A_1^* A_1\delta A_1,\\
\delta\dot{A}_2 &= -\frac{\kappa}{4\omega_2}f(t)\delta A_1^* - i\frac{\varepsilon}{\omega_2}B_1\delta B_1 - \frac{1}{2}\alpha_2\delta A_2\\
&-\frac{3}{2}\omega_2^2\beta_2 A_2^2\delta A_2^* - 3\omega_2^2\beta_2 A_2^* A_2\delta A_2,\\
\delta\dot{B}_1 &= -\frac{\kappa}{4\omega_1}f(t)\delta B_2^* - i\frac{\varepsilon}{\omega_1}(A_2\delta B_1^* + B_1^*\delta A_2)\\
&-\frac{1}{2}\alpha_1\delta B_1 - \frac{3}{2}\omega_1^2\beta_1 B_1^2\delta B_1^* - 3\omega_1^2\beta_1 B_1^* B_1\delta B_1,\\
\delta\dot{B}_2 &= -\frac{\kappa}{4\omega_2}f(t)\delta B_1^* - i\frac{\varepsilon}{\omega_2}A_1\delta A_1 - \frac{1}{2}\alpha_2\delta B_2\\
&-\frac{3}{2}\omega_2^2\beta_2 B_2^2\delta B_2^* - 3\omega_2^2\beta_2 B_2^* B_2\delta B_2.
\end{aligned} \tag{11}$$

Each time after a certain number of integration steps have been performed, the Gram–Schmidt orthonormalization process is applied to the perturbation vectors $\{\delta A_1', \delta A_1'', \delta A_2', \delta A_2'', \delta B_1', \delta B_1'', \delta B_2', \delta B_2''\}$.

The Lyapunov exponents are calculated by averaging the growth rates of the sum of logarithms of norms of the perturbation vectors after orthogonalizing, but before normalizing, them. The Lyapunov spectrum cal-

[3] The phase cannot be defined globally on the entire time axis, because the amplitude is nearly zero when the subsystem is idle. If such a definition were possible, then the first-return map for the phase might not belong to the appropriate topological class.

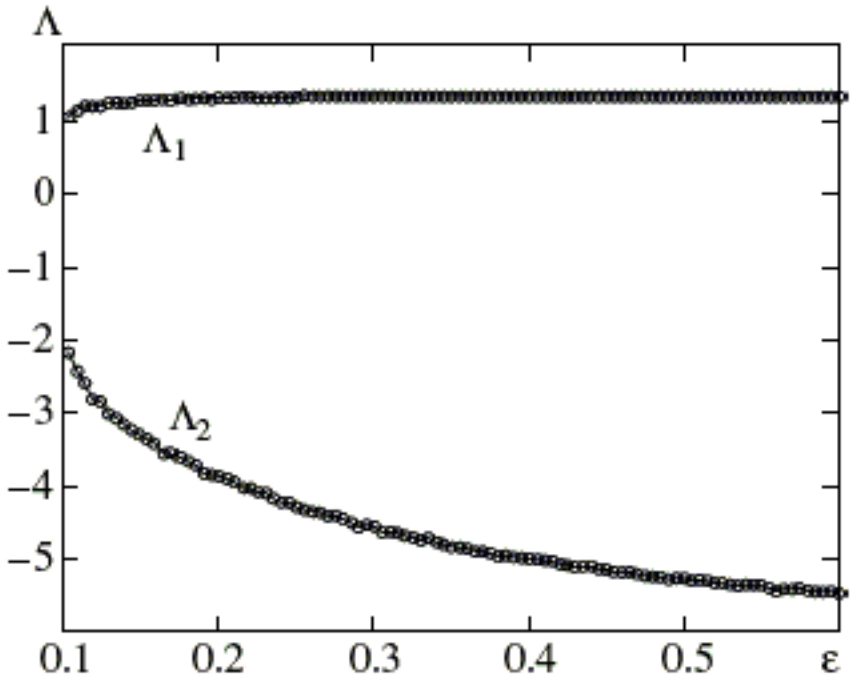

Fig. 4. The largest two Lyapunov exponents of stroboscopic Poincaré map vs. parameter ε computed for $\omega_1 = 2\pi$, $\omega_2 = 4\pi$, $\omega_3 = 6\pi$, $T = 40$, $\kappa = 35$, $\alpha_1 = \alpha_2 = 0.6$, and $\beta_1 = \beta_2 = 0.01$. The largest exponent is consistent with the estimated $\Lambda_1 \approx \ln 4$.

culated for the attractor corresponding to parameter set (10) is as follows:

$$\begin{aligned}
\lambda_1 &= 0.03456 \pm 0.00006,\\
\lambda_2 &= 0.1320 \pm 0.0003,\\
\lambda_3 &= -0.2247 \pm 0.0004,\\
\lambda_4 &= -0.5220 \pm 0.0004,\\
\lambda_5 &= -0.6826 \pm 0.0008,\\
\lambda_6 &= -0.9012 \pm 0.0018,\\
\lambda_7 &= -1.4189 \pm 0.0004,\\
\lambda_8 &= -2.3248 \pm 0.0007.
\end{aligned} \qquad (12)$$

The corresponding Lyapunov exponents of the stroboscopic Poincaré map are determined from (12) as $\Lambda_k = \lambda_k T$. In particular, $\Lambda_1 = 1.3823 \pm 0.0023$, which is in good agreement with the value $\ln 4 = 1.3862\ldots$ obtained by using the Bernoulli-type map $\varphi_{n+1} = 4\varphi_n + \text{const} \pmod{2\pi}$ for the phase variable.

A positive Λ_1 is an indicator of chaos. Since the remaining exponents $\Lambda_2, \ldots, \Lambda_8$ are negative, only one eigendirection in the phase space of the Poincaré map is expanding and the remaining ones are contracting.

Figure 4 shows the two highest Lyapunov exponents of the Poincaré map calculated as functions of the coupling strength ε while the remaining parameters are held constant. The positive exponent smoothly depends on the parameter and has no sharp dips characteristic of nonhyperbolic attractors. It is clear from Fig. 4 that the value of Λ_1 is close to $\ln 4$ over a wide interval of ε.

The Kaplan–Yorke dimension [6, 8, 21, 28] of the attractor of the stroboscopic Poincaré map with Lyapunov spectrum (12) is

$$D = 1 + \Lambda_1/|\Lambda_2| \approx 1.26 \qquad (13)$$

(since $\Lambda_1 > 0$ and $\Lambda_1 + \Lambda_2 < 0$). Accordingly, the total dimension of the attractor embedded in the 9D extended phase space is $D' = D + 1 \approx 2.26$.

Figure 5a shows Poincaré section of the phase portrait of the attractor obtained by projection onto the phase plane of oscillator *1* in subsystem B. Figure 5b shows an enlarged fragment of Fig. 5a to illustrate some details of the transverse fractal structure of the attractor. Figure 5c shows an analogous phase portrait corresponding to a coupling strength value near the threshold for existence of the chaotic attractor, where the transverse fractal structure is more visible.

4. DISCUSSION: THE HYPERBOLICITY HYPOTHESIS

The principle of operation of the parametric hyperbolic chaos generator considered here and its numerical realization suggest that the observed chaotic attractor is uniformly hyperbolic.

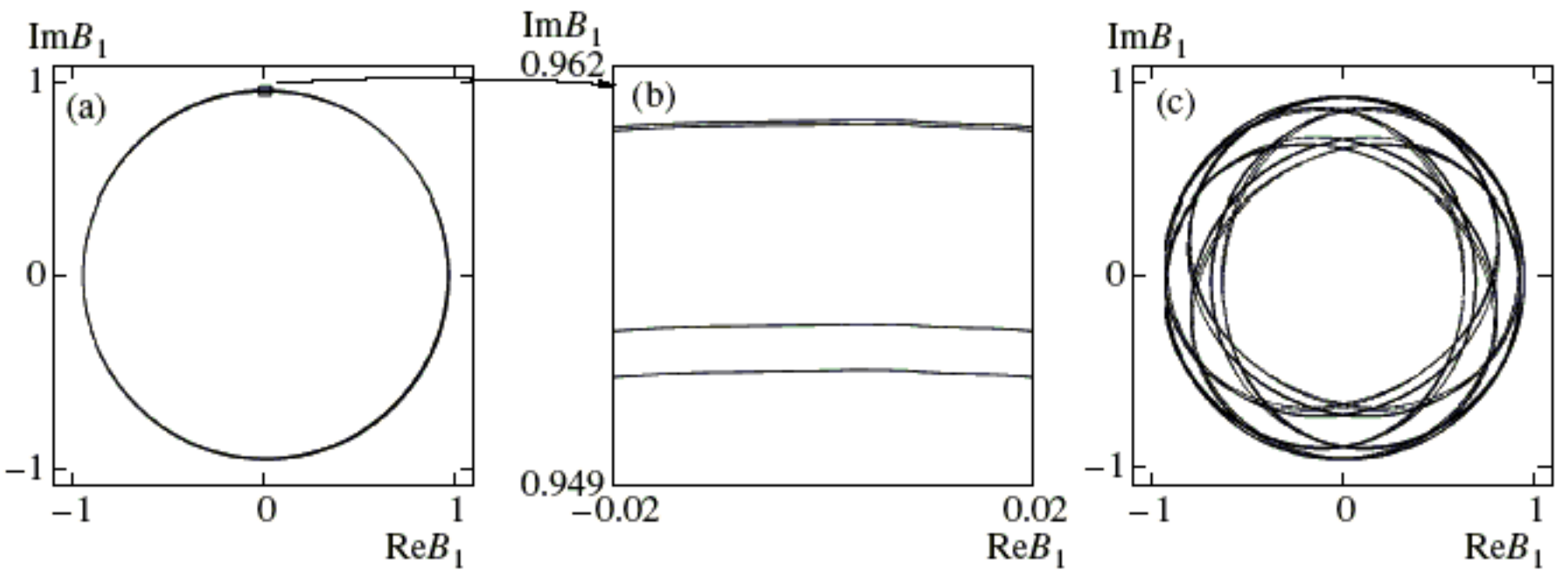

Fig. 5. Poincaré section of the attractor portrait projected onto the complex amplitude plane of oscillator *1* in subsystem B for ε = 0.5 (a) and 0.125 (c); (b) an enlarged fragment of (a).

Following the analysis developed by Shil'nikov and Turaev in a somewhat different context [5, 29], define phase space coordinates $\mathbf{X}_n = \{\mathbf{x}_n, \varphi_n\}$ as

$$\mathbf{x}_n = \{A_1', A_1'', A_2', A_2'', |B_1|, B_2', B_2''\} \in \mathbb{R}^7,$$

$$\varphi_n = \arg B_1|_{t=nT} \in S,$$

where $\mathbb{R}^7$ is the 7D Euclidean space and S is the one-dimensional circle. Then, Poincaré map (9) can be represented as

$$\begin{aligned} \mathbf{x}_{n+1} &= \mathbf{f}(\mathbf{x}_n, \varphi_n), \\ \varphi_{n+1} &= m\varphi_n + g(\varphi_n) + \omega + h(\mathbf{x}_n, \varphi_n) \pmod{2\pi}. \end{aligned} \tag{14}$$

Here, m is an integer ($m = 4$ for the system under study); ω is a constant number in $[0, 2\pi)$; and $\mathbf{f}$, g, and h are smooth functions 2π-periodic in φ. If $\mathbf{f}$ and h are functions with sufficiently small norms, then (14) can be approximated by the map

$$\mathbf{x}_{n+1} = 0, \quad \varphi_{n+1} = m\varphi_n + g(\varphi_n) + \omega \pmod{2\pi}. \tag{15}$$

Furthermore, according to [5, 29], if $m \geq 2$ and $|m + g'(\varphi)| > 1$, then map (14) has an attractor topologically equivalent (homeomorphic) to the Smale–Williams solenoid. In the spirit of the standard mathematical terminology, the original flow is said to have an attractor topologically equivalent to a suspension of the Smale–Williams' solenoid.

Most importantly, $m = 4$ in (14) implies that the map belongs to the appropriate topological class, as illustrated by Fig. 3.

The branch pattern in the figure, as well as the proximity of the largest Lyapunov exponent of the Poincaré map to $\Lambda_1 \approx \ln 4$, suggests that the condition $|m + g'(\varphi)| > 1$ is satisfied.

Since the Lyapunov exponents $\Lambda_2, \ldots, \Lambda_8$ are negative and large in absolute value as compared to Λ_1, the functions $\mathbf{f}$ and h in (14) must have sufficiently small norms.

As a geometrical interpretation of the stroboscopic Poincaré map, consider a 8D solid toroid (the direct product of a one-dimensional circle with a 7D ball). At each step of the map, it is stretched to four times its original length, contracted in the transverse direction, folded in four, and squeezed into its original volume. Thus, the winding number of the map is 4. As the process is continued ad infinitum, an attractor of Smale–Williams solenoid type is generated, with a cross section similar to the Cantor set.

Evidence of the uniform hyperbolicity of the attractor could be obtained by using the numerical procedure described in [14, 15] to verify certain conditions for the expanding and contracting cones in the tangent spaces at points inside a bounded phase-space domain containing the attractor [1, 6]. However, the computational complexity of this procedure applied to the system in question would be too high, because the corresponding phase-space dimension of the Poincaré map is as high as 8 (cf. an analogous dimension of 4 in [14, 15]).

Even though the hyperbolicity of the chaotic attractor is only hypothetical, the parametric chaos generator considered here is of interest in its own right, because its performance is robust under the choice of parameters and components of its electronic, mechanical, acoustical, or nonlinear optical implementations. In particular, parametric generators can be used in chaos-based secure communication systems, which are currently the subject of extensive discussion [30].

ACKNOWLEDGMENTS

I thank N.M. Ryskin for a helpful discussion. This work was supported by the Russian Foundation for Basic Research, project no. 06-02-16773.

REFERENCES

1. Ya. G. Sinaĭ, in *Nonlinear Waves* (Nauka, Moscow, 1979), p. 192 [in Russian].
2. *Modern Problems of Mathematics. Fundamental Directions. Scientific and Technical Results*, Ed. by R. V. Gamkrelidze (VINITI, Moscow, 1985), Vol. 2 [in Russian].
3. J.-P. Eckmann and D. Ruelle, Rev. Mod. Phys. **57**, 617 (1985).
4. R. L. Devaney, *An Introduction to Chaotic Dynamical Systems* (Addison-Wesley, New York, 1989).
5. L. Shilnikov, Int. J. Bifurcations Chaos **7**, 353 (1997).
6. A. B. Katok and B. Hasselblatt, *Introduction to the Modern Theory of Dynamical Systems* (Cambridge Univ. Press, Cambridge, 1995; Factorial, Moscow, 1999).
7. V. Afraimovich and S.-B. Hsu, *Lectures on Chaotic Dynamical Systems* (Am. Math. Soc., Providence, RI, 2003), AMS/IP Studies in Advanced Mathematics, Vol. 28.
8. J. Guckenheimer and P. J. Holmes, *Nonlinear Oscillations, Dynamical Systems and Bifurcation of Vector Fields* (Springer, Berlin, 1990; Inst. Komp'yut. Issled., Moscow–Izhevsk, 2002).
9. V. S. Anishchenko, V. V. Astakhov, T. E. Vadivasova, A. B. Neĭman, G. I. Strelkova, and L. Schimansky-Geier, *Nonlinear Effects of Chaotic and Stochastic Systems* (Inst. Komp'yut. Issled., Moscow, 2003) [in Russian].
10. V. Belykh, I. Belykh, and E. Mosekilde, Int. J. Bifurcations Chaos **15**, 3567 (2005).
11. T. J. Hunt and R. S. MacKay, Nonlinearity **16**, 1499 (2003).
12. S. P. Kuznetsov, Phys. Rev. Lett. **95**, 144101 (2005).
13. S. P. Kuznetsov and E. P. Seleznev, Zh. Éksp. Teor. Fiz. **129**, 400 (2006) [JETP **102**, 355 (2006)].
14. S. P. Kuznetsov and I. R. Sataev, Izv. Vyssh. Uchebn. Zaved., Prikl. Nelin. Din. **14** (5), 3 (2006).
15. S. P. Kuznetsov and I. R. Sataev, Phys. Lett. A **365**, 97 (2007).
16. O. B. Isaeva, A. Yu. Jalnine, and S. P. Kuznetsov, Phys. Rev. E **74**, 046207 (2006).

17. P. V. Kuptsov and S. P. Kuznetsov, Nelin. Din. **2**, 307 (2006).
18. O. B. Isaeva, S. P. Kuznetsov, and A. N. Osbaldestin, Pis'ma Zh. Tekh. Fiz. **33** (17), 69 (2007) [Tech. Phys. Lett. **33**, 748 (2007)].
19. S. P. Kuznetsov and A. S. Pikovsky, Physica D (Amsterdam) **232**, 87 (2007).
20. L. I. Mandel'shtam, *Lectures on Oscillations* (Akad. Nauk SSSR, Moscow, 1955) [in Russian].
21. M. I. Rabinovich and D. I. Trubetskov, *Introduction to the Oscillation and Wave Theory* (Nauka, Moscow, 1984) [in Russian].
22. W. H. Louisell, *Coupled Mode and Paramagnetic Electronics* (Wiley, New York, 1960; Inostrannaya Literatura, Moscow, 1963).
23. A. P. Kuznetsov, S. P. Kuznetsov, and N. M. Ryskin, *Nonlinear Oscillations* (Fizmatlit, Moscow, 2005) [in Russian].
24. F. R. Gantmakher, *Lectures on Analytic Mechanics* (Nauka, Moscow, 1966) [in Russian].
25. P. Gaspard, in *Encyclopedia of Nonlinear Science* (Routledge, New York, 2005), p. 548.
26. V. I. Arnol'd, *Ordinary Differential Equations* (Nauka, Moscow, 1971; MIT Press, Cambridge, Mass., 1973).
27. G. Bennetin, L. Galgani, A. Giorgilli, and J.-M. Strelcyn, Meccanica **15**, 9 (1980).
28. S. P. Kuznetsov, *Dynamical Chaos* (Fizmatlit, Moscow, 2001) [in Russian].
29. L. P. Shil'nikov and D. V. Turaev, Dokl. Akad. Nauk **342**, 596 (1995).
30. A. S. Dmitriev and A. I. Panas, *Dynamic Chaos: New Information Carriers for Communication Systems* (Fizmatlit, Moscow, 2002) [in Russian].

Translated by A. Betev